

# Modifying Polyester Surfaces with Incompatible Polymer Additives

Reactive and Functional Polymers ., 03/2015; DOI: 10.1016/j.reactfunctpolym.2015.03.002

Christopher D. James,<sup>1</sup> Christopher Jaynes,<sup>2</sup> Nuno P. Barradas,<sup>3</sup> Luke Clifton,<sup>4</sup> Robert M. Dalgliesh,<sup>4</sup> Rebecca F. Smith,<sup>1,5</sup> Stephen W. Sankey,<sup>6</sup> Lian R. Hutchings<sup>1</sup> and Richard L. Thompson.<sup>1\*</sup>

<sup>1</sup> Department of Chemistry, Durham University, Mountjoy Site, Durham, DH1 3LE, U.K.

<sup>2</sup> University of Surrey Ion Beam Centre, Guildford, GU2 7XH, U.K.

<sup>3</sup> Instituto Superior Técnico, E.N. 10 ao km 139,7, 2695-066 Bobadela LRS, Portugal

<sup>4</sup> STFC ISIS Neutron and Muon Facility, Rutherford Appleton Laboratory, Chilton, Didcot, Oxfordshire OX11 0QX, U.K.

<sup>5</sup> Current address: School of Chemical Engineering and Analytical Science, The University of Manchester, Oxford Road, Manchester, UK, M13 9PL

<sup>6</sup> DuPont Teijin Films Ltd., Wilton Centre, Middlesbrough, Teesside, TS90 8JE, U.K.

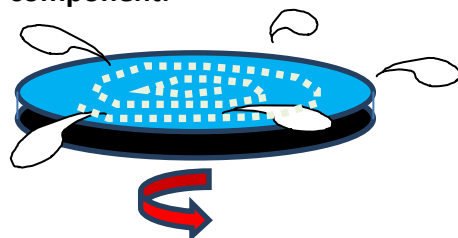
\*To whom correspondence should be addressed:

Email [r.l.thompson@dur.ac.uk](mailto:r.l.thompson@dur.ac.uk)

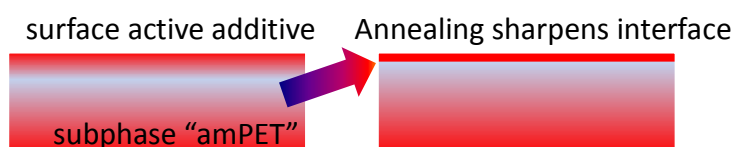
Tel +44 191 3342139

Fax +44 191 3844737

**Spin cast films of incompatible polymers consistently yield a macromolecular monolayer of the surface active component.**



**Film profiles**



## Abstract

Surface modification of amorphous PET in incompatible blends is demonstrated using fluorocarbon end-functional polystyrenes. Contact angles with water and decane were consistent with high levels of surface fluorocarbon, even for spin-cast films with no further processing required. Hydrophobicity and lipophobicity were further increased by annealing above the glass transition temperature. High resolution depth profiling using complementary ion beam analysis and specular neutron reflectometry has enabled accurate characterisation of the composition profile of the additive including the minimum in additive concentration found just below the surface enriched layer. This analysis quantified the very low compatibility between the modifying polymer and the amorphous PET and was consistent with the highly segregated nature of the adsorbing species and its sharp interface with the subphase. For these incompatible polymer blends, surfaces enriched with the surface active polymer could coexist at equilibrium with extremely low (~0.4 %) bulk

loadings of the additive. This suggests that for thicker films at even lower additive concentrations than the minimum 1% that we studied, it may be possible to achieve efficient surface modification. However, at this concentration, the efficiency of surface modification is limited by the processing conditions. Finally we note that in higher loadings of surface active additive there is clear evidence for lateral phase separation into patterned domains of differing composition. The enhancement in surface properties is due to local reorganisation rather than bulk redistribution of the components within the film, as the composition versus depth distributions of the polymer blend components was observed to be relatively unaffected by annealing.

## Introduction

A continuing challenge for the polymer industry is to deliver new effects or enhanced properties from a palette of materials that is often increasingly restricted. For example, in food and drug applications a limited range of approved materials exists, which may be used in applications where they are to be ingested, or in contact with materials that are ingested. For many other applications, sophisticated tooling and production methods, which have been developed and commercialised over decades are prohibitively expensive to adapt for entirely new polymers. With rising raw materials cost, and growing concern over environmental impact, there is a continuing drive to “do more with less”, and to achieve this with existing production facilities. For these reasons, it is often more appealing to modify an existing polymer than it is to attempt to synthesize an entirely class of materials.

Surface modification is a clear example where desirable improvements in performance, for example biocompatibility,<sup>1</sup> hydrolysis or wear resistance<sup>2</sup> are obtainable and enable new applications for existing polymers. For most applications, it is vital for this to be achieved without altering the bulk properties that are compatible with established processing protocols. In recent years, we have shown that the controlled introduction of multiple functional groups the ends of polymer chains allows these materials to be added to a compatible matrix.<sup>3</sup> The functional groups can be sufficiently surface-active to achieve dramatic surface modification. “PTFE-like” surfaces can be generated on many polymers whilst retaining their other desirable bulk properties of these polymers, as defined by their solubility, melting temperature and glass transition temperature.<sup>3-6</sup> Until now, work on surface modification with end functional polymers has focused almost exclusively on blends in which the matrix polymer and the end-functionalised polymer chain are compatible. Increasingly, it is becoming recognised that more complex, multiphase polymer blends and composites offer distinct advantages over single phase materials. It is well known, for example, that the presence of separate phases can offer much greater control over bulk properties (e.g. modulus, glass transition temperature) than is possible with single phase blends.<sup>7</sup> However, there are relatively few reports in the literature on the surface modification of polyesters by functional polymers, and most have focused on the biodegradable polyesters. Esteves *et al* have recently demonstrated the potential of

oligomeric fluorocarbon functionalised PCL to modify the surface of a cross-linked resin,<sup>8</sup> and that the inclusion of appropriately functionalised particles in polymers has enabled the formation of durable, recoverable superhydrophobic coatings.<sup>9</sup> In our own earlier work,<sup>10</sup> we found that multi-fluorocarbon end functional polylactides could confer highly hydrophobic surfaces to compatible blends with polylactides, which would otherwise be quite hydrophilic, and Abe *et al*<sup>11</sup> demonstrated that end functional polylactides could significantly increase the stability of polylactides with respect to enzymatic degradation.

Due to their relatively high cost, efficient use of surface modifying additives is essential. Therefore, a clear understanding of the influences of key parameters such as degree of functionalisation, molecular weight, or process conditions is necessary to successfully implement the use of functional polymer additives to achieve surface modification. Hydrophobicity is determined by topography as well as surface chemistry, so spurious results occur when a surface is inadvertently roughened or contaminated. Furthermore, only by understanding the equilibrium between bulk and surface concentration and the approach to this state is it possible to predict the most cost-efficient combination of additive concentration, process time and temperature to deliver the required level of surface modification. Therefore, validation of this technology depends not only on characterisation by standard techniques such as contact angle analysis, but more sophisticated methods that can probe beneath the surface are also essential to understand the mobility<sup>5</sup> and efficiency<sup>4</sup> of surface adsorption of the functional additive. This is a significant challenge to address since it is necessary to quantify behaviour on length scales comparable to polymer chain dimensions (typically 3-30 nm) as well as the much larger scales associated with diffusion and phase separation (0.1-10  $\mu\text{m}$ ).<sup>12-15</sup> Many methods can achieve or even exceed the required depth resolution near surfaces (ToF-SIMS,<sup>16</sup> XPS,<sup>17</sup> neutron reflection<sup>18</sup>, etc) and there are also methods such as confocal microscopy<sup>19,20</sup> that can deliver the range required for phase separation or stratification. However, ion beam analysis appears to be almost the only technique in which it is possible to span the relevant depth range with sufficient resolution in a single experiment.<sup>21,22</sup>

Here we compare the influences of functionality and incompatibility for the first time in a multi-end functional polymer blend, which has been designed to deliver hydrophobic surfaces. Such surfaces might be expected to enhance the hydrolytic stability of polyester, which would improve the lifetime of polyester film in many applications. The viability of this concept has been demonstrated by the work by Abe *et al*<sup>11</sup> mentioned earlier, but we are unaware of any equivalent work being carried out on PET.

Our test system is based on a multi-fluorocarbon end-functional polystyrene, which is known to be extremely surface active in polystyrene matrices. However the surface behaviour of this type of additive in a less compatible matrix has not previously been explored, and is not trivial to predict. This blend has significant practical interest, since increasing the hydrophobicity of polyester has the potential to improve resistance to

hydrolysis, but only if the additive could migrate to the blend surface and furthermore, that the hydrophobic layer has sufficient mechanical stability to remain on the blend surface. The possibility of achieving surface modification with very low quantities of an incompatible surface active polymer is extremely desirable, since it greatly increases the potential utility of this class of additive material as well as the other industrially important polymers such as PEN, PP and PE for which surface modification is desirable. We explore the separate influences of multiple fluorocarbon functionality and matrix incompatibility on the surface properties of spin cast blended films. The vertical depth distribution of the additives responsible for surface modification is analysed in detail using complementary ion beam analysis for the main features of the profile, and neutron reflectometry to explore the fine structure of the adsorbed layer and the influence of annealing on this structure. Finally, we consider the impact of matrix incompatibility on the lateral homogeneity of a blended film surface and show that even for low surface energy additives that can appear to yield a surface wetting layer, lateral phase separation may occur.

## Experimental

A tri-fluoro end functional deuterated polystyrene ( $M_n = 11.2$  kg/mol,  $M_w = 14.9$  kg/mol) ("3CFdPS11") was prepared by living radical polymerisation of dPS from a fluorocarbon functionalised initiator. Each fluorocarbon functional  $C_8F_{17}$  group, has a length of approximately  $1$  nm<sup>10</sup> and a cross-sectional area of approximately  $0.28$  nm<sup>2</sup>,<sup>23</sup> and therefore accounts for approximately 5% of the volume of the 3CFdPS11 chain. The synthetic methodology ensured that all of the polymer chains carried the fluorocarbon functional groups and that there was good control over the final molecular weight distribution. Further details of the synthesis are given in an earlier publication.<sup>6</sup> An unfunctionalised deuterium labelled polystyrene of similar molecular weight, dPS11, ( $M_n = 11.1$  kg/mol,  $M_w = 11.4$  kg/mol) was also prepared as a control additive to enable the influence of the fluorocarbon functionality on the material properties to be isolated. An amorphous polyester was prepared by condensation polymerisation of bishydroxyethylterephthalate (BHET) and bishydroxyethylisophthalate (BHEI) in a 3:2 ratio as shown in figure 1. The reaction, yields a random copolymer, poly(ethyleneterephthalate-*r*-ethyleneisophthalate), which is an amorphous analogue to semi-crystalline poly(ethyleneterephthalate), PET.<sup>24</sup> The absence of any detectable melting transition, and therefore the absence of crystalline domains, was confirmed by differential scanning calorimetry, and we refer to this material hereafter as "amPET". The molecular weight distribution of the resulting amPET was characterised by GPC using chloroform as the solvent. The number average molecular weight,  $M_n$ , was 5600 g/mol and the polydispersity index,  $M_w / M_n$  was 5.6. A further control sample of hydrogenated polystyrene, hPS100,  $M_n = 90\ 000$  g mol<sup>-1</sup>,  $M_w/M_n = 1.10$ , was used in order to resolve the effects of matrix incompatibility on the surface properties.

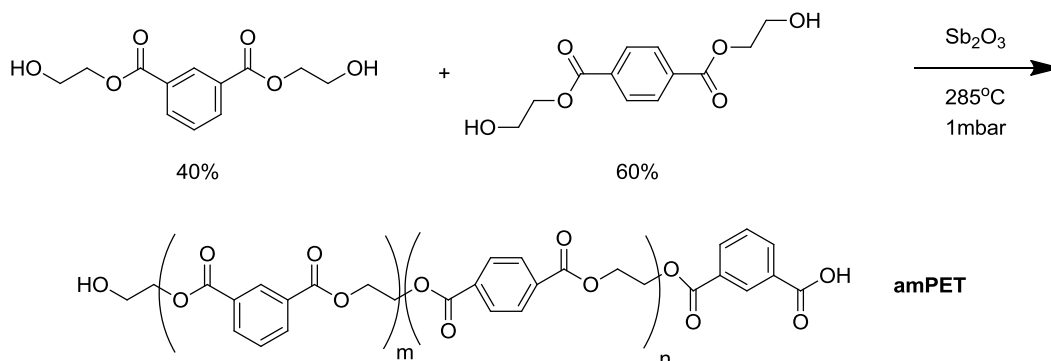


**Figure 1: Reaction scheme for the synthesis of amPET**

Polymer blend films were prepared by co-dissolution of the constituent polymers in their required proportion in chloroform so that the total polymer concentration in the solution was approximately 4% (w/w). These solutions were spin-cast onto clean silicon wafers using a photoresist spinner at  $\sim 2500$  rpm for 25 s to yield smooth films of approximately 500 nm total thickness. Prior to solution spin casting, wafers were split into  $2\text{ cm} \times 2\text{ cm}$  squares, which were cleaned of any debris and surface contamination by repeated spin-casting of pure toluene (99+%) at 3200 rpm. After allowing sufficient time for the solvent to evaporate, the films were analysed in this ‘unannealed’ state, or were annealed in a vacuum oven at  $160^\circ\text{C}$  for 1 hour.

Static contact angle analysis was carried out using a Ramé-Hart NRL manual goniometer (100-00-230) using high purity water and n-decane as the contacting fluids. The use of a polar and non-polar contact fluid enabled an approximate measure of surface energy to be derived using the Owens-Wendt method.<sup>25</sup> More importantly the use of a non-polar contact fluid also enables the direct confirmation of the presence of significant levels of fluorocarbon on the film surface, since decane wets both PS and PET giving almost zero contact angles in the absence of fluorocarbon.

An NEC 5SDH Pelletron accelerator was used for ion beam analysis (IBA) experiments. A 2.4 mm diameter beam of  $^3\text{He}^+$  ions, 0.7 MeV, 4  $\mu\text{C}$  total charge was incident on each sample. Measurements were carried out at grazing incidence to ensure sufficient depth resolution to quantify the surface excess of the deuterium labelled additive. The energetic nuclear reaction products arising from the  $\text{D}(^3\text{He},\text{p})\alpha$  reaction ( $Q = 18.353\text{ MeV}$ )<sup>26</sup> were detected at  $170^\circ$  to the incident beam. Both protons and alphas are detected, but the protons carry the most information: the PIPS detector had an active layer 1.5 mm thick, and an energy resolution of approximately 19 keV.

Specular neutron reflectivity experiments were carried out at the SURF reflectometer, ISIS neutron Source, Rutherford Appleton Laboratories, UK. Samples were prepared in the same way as for ion beam analysis except that they were spin cast onto 5 mm thick, 50 mm diameter silicon blocks, from a 2% w/w polymer solution in order to yield films of approximately 100 nm thick. Reflectivity data were collected over the range  $0.005 < Q / \text{\AA}^{-1} < 0.3$ , which covers the range from critical reflectivity to the background.

In this work the IBA profiles were first fitted without presupposing any theoretical model, and then fitted with the functional form specified in Eq.2 using the DataFurnace code<sup>27</sup> with the executable NDFv9.6a. The methodology is described in greater detail elsewhere, and is summarised in the supporting information (S.I.1)<sup>282530</sup>. Model-free fitting is necessary to demonstrate that the assumed model is valid for these data, but a relatively coarse layer structure is the natural output because of the intrinsic depth resolution of the technique. The knowledge that the profile is not discontinuous is extra prior information that is not objectively in the IBA data. The model-free fit could of course be improved, but then would for our present purposes have to be parameterised. Figure 4 shows the difference between a model-free fit and the fitted model: the issue of how to extract maximum information from the data, with Bayesian and other methods, is discussed at length by Jeynes *et al*<sup>31</sup>.

## Results

### ***Surface modification of PET and PS by end-functional polystyrenes.***

Figure 2(a) shows the results of contact angle analysis with water on a variety of blended polymer films. We note that the behaviour observed in these spin-cast films is quite similar to that reported previously for compatible blends in which the functional polymer additive and matrix polymer had the same repeat unit.<sup>3-6</sup> At low concentrations of additive there is a sharp increase in hydrophobicity with increasing additive concentration up to a plateau value typically obtained at approximately 2-4 % additive. For the control additive, dPS11, which lacks any fluorocarbon groups, the maximum contact angle obtained is not much more than 90°, consistent with the value obtained for the unmodified hPS100 film, and our previous results for contact angles on unmodified polystyrene surfaces.<sup>3,6</sup> In contrast, the presence of 3 C<sub>8</sub>F<sub>17</sub> fluorocarbon groups per chain end of the 3CFdPS11 additive is sufficient to yield contact angles well in excess of 100°, and at higher loadings (>4% w/w) approach values expected for PTFE. We note that although the 3CFdPS11 has more CF<sub>3</sub> groups than PTFE, the hydrophobicity does not exceed that of PTFE because each functional group is covalently bound to a much larger hydrocarbon chain, and it is unlikely that sufficient packing density could ever be achieved to present a pure CF<sub>3</sub> surface. As seen previously for pure PS films, annealing above the glass transitions of the constituent polymers gives a further increase in hydrophobicity for any given additive concentration. Since our results for both additives in PET, an incompatible matrix, are rather similar to those for the hPS100

matrix, with which the additives are fully compatible, our contact angle results strongly suggest that incompatibility has relatively little influence on surface activity of functional polymers. Only at low concentrations where there is insufficient additive to achieve high surface coverage, do our results diverge toward the values expected for the unmodified matrix materials.

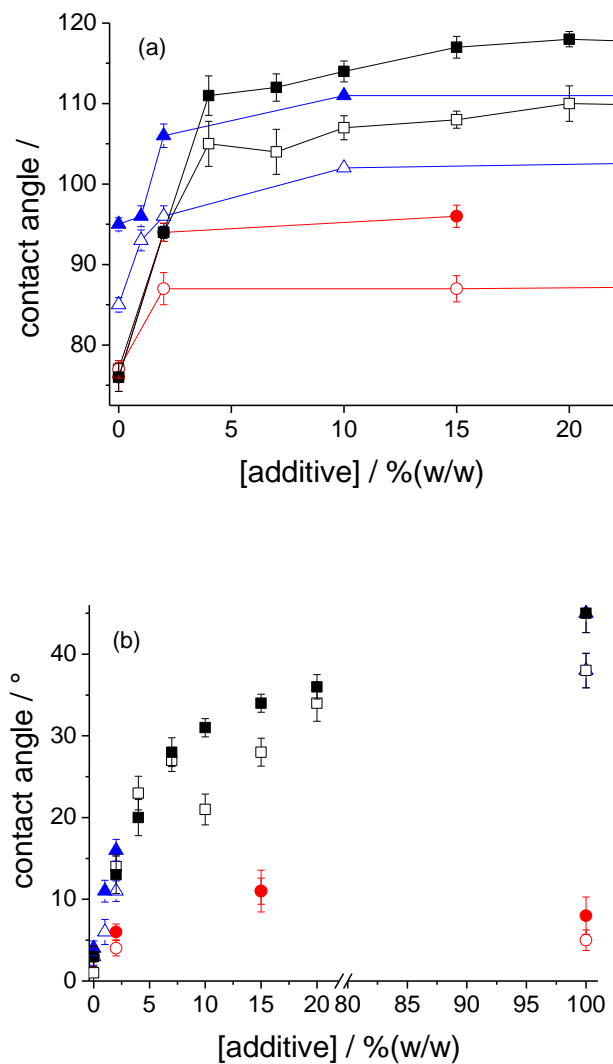


**Figure 2.** Influence of 3CFdPS11 additive concentration on the contact angle of (a) water and (b) n-decane in hPS100 (triangles) and in amPET (squares). Data for a control experiment DPS in amPET are included as circles. Contact angles measured before annealing are shown as open symbols and after annealing as solid symbols. The lines are a guide to the eye and include interpolation to measurements made at 100% additive.

Although it is not expected that sample roughness could contribute significantly to the measured changes in hydrophobicity in smooth spin-cast films, we cannot reject this

possibility based on the aqueous contact angle analysis data alone. However, in all of our blended films containing 3CFdPS11, a qualitatively similar trend in contact angle was observed for nonpolar n-decane as were found with water. Results for n-decane contact angle experiments are shown in figure 2(b). This is a significant observation in that even relatively rough surfaces of the unmodified PET or PS should yield decane contact angle of approximately zero. On this basis, the existence of significant (up to 45°) contact angles with a nonpolar contact fluid provides clear evidence of a fluorocarbon enriched surface.

Using the Owens-Wendt model, we can estimate the modified surface energy from the contact angle,  $\theta$ , obtained with multiple contact fluids.

$$\cos \theta = \frac{2\sqrt{\sigma_S^D \sigma_L^D}}{\sigma_L} + \frac{2\sqrt{\sigma_S^P \sigma_L^P}}{\sigma_L} - 1 \quad (1)$$

where the total surface tension of the contacting fluid,  $\sigma_L$ , can be separated into its polar ( $\sigma_L^P$ ) and dispersive ( $\sigma_L^D$ ) contributions, and the total solid surface energy, which is the parameter of interest to determine, is given by the sum of its polar and dispersive components,  $\sigma_S^P$  and  $\sigma_S^D$  respectively. Two probe liquids – deionized water ( $\sigma_L = 72.8$  mN/m;  $\sigma_L^D = 21.8$  mN/m,  $\sigma_L^P = 51.0$  mN/m) and n-decane, ( $\sigma_L = 23.8$  mN/m;  $\sigma_L^D = 23.8$  mN/m,  $\sigma_L^P = 0$  mN/m), yield two equations from which the two unknown parameters,  $\sigma_S^D$  and  $\sigma_S^P$ , can be determined. Although absolute values obtained in this way should be treated with caution, the overall trend shown in figure 3 is credible and shows that there is a systematic reduction in surface energy with increasing additive concentration, which is most apparent for the fluorocarbon functionalised additive, and becomes somewhat more dramatic after the samples have been annealed above the glass transition temperature of the components.

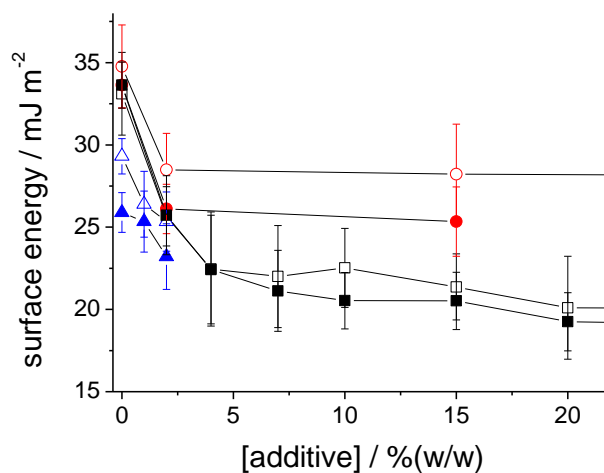


**Figure 3. Surface energy of blended films as a function of composition and annealing. Notation is the same as for figure 2.**

In the first instance to fit the NRA data, the additive concentration profile was approximated by a series of discrete layers of varying composition, and the calculated proton spectra were iteratively fitted from an initial simulation to the measured spectra by varying the thickness and composition of each layer. The minimum layer thickness was set to  $5 \times 10^{16}$  atoms/cm<sup>2</sup>, which for our materials is approximately 5 nm and was chosen to be similar to the instrumental depth resolution at the lowest grazing angle of incidence employed. This approach has been successfully used to characterise the surface segregation of deuterium labelled polymer previously.<sup>29</sup> In subsequent fits, the layer model was replaced with the analytical functional form given by equation 2,

$$\phi(z) = \frac{1}{2} \left( 1 + \operatorname{erf} \frac{h_1 - z}{w_1} \right) + \frac{\phi_b}{2} \left( 1 + \operatorname{erf} \frac{z - h_2}{w_2} \right) \quad (2)$$

where  $h_1$  is the thickness of the surface enriched layer and  $w_1$  is the width of the interface between this layer and the adjacent concentration, which is expected to be somewhat depleted with respect to the bulk concentration,  $\phi_b$ . A gradual increase in concentration between the depleted layer and the bulk is also expected, which is represented by the corresponding parameters in the second term of equation 2. NRA data for 10% 3CFdPS11 in amPET are shown in figure 4, along with the fits to the experimental data obtained using the layer and analytical function models. The vertical composition profiles obtained by each fitting method are compared in figure 5.

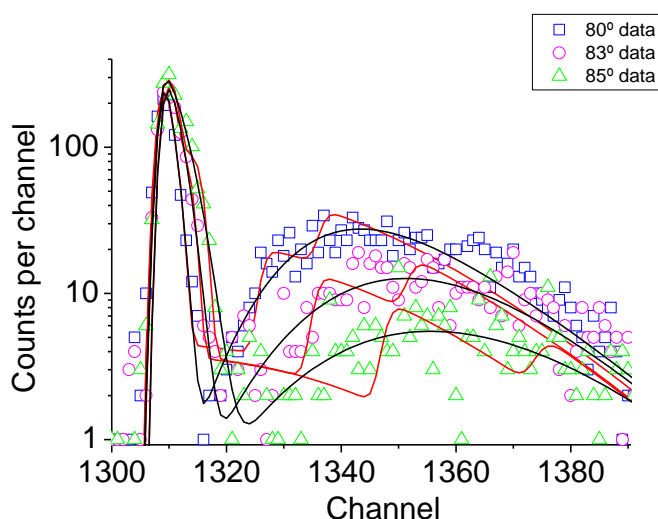


**Figure 4. Simultaneous self-consistent fits of IBA data at three beam incident angles. Data and fits (lines) for layer model (red) and obtained using equation 2 (black) to determine the concentration profile of the 3CFdPS11 additive.**

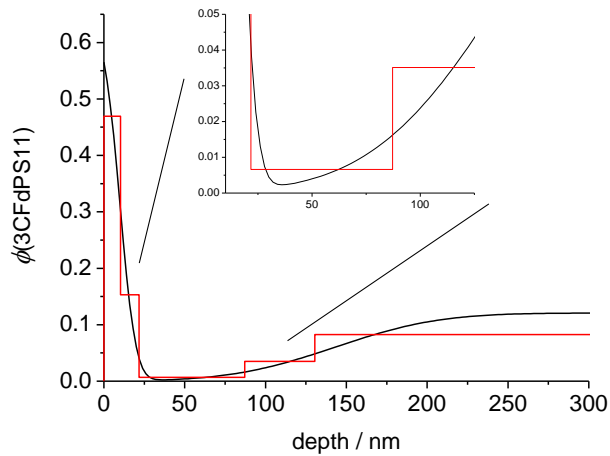


**Figure 5. Comparison of concentration profiles obtained by layer models (red) and a functional form model (black). The inset highlights the composition profile determined in the depleted region below the surface.**

Control NRA experiments were also carried out, at a single angle of incidence, to isolate the contributions to the vertical depth distribution of each deuterium labelled additive arising from matrix incompatibility and fluorocarbon functional groups. Data and fits are included as supporting information S.I.2. The composition versus depth profiles obtained using equation 2 are presented in figure 6. It is evident that with the exception of dPS11 in hPS100, (which is only expected to be significantly surface active at much higher molecular weights than are considered here)<sup>30</sup>, all of the other spin-cast films show a considerable level of additive surface segregation.

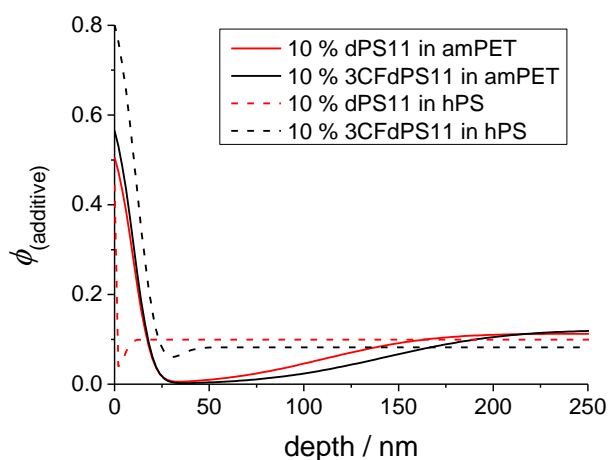


**Figure 6. Influences of matrix compatibility and fluorocarbon functionality on the depth distribution of spin-cast films comprising 10% additives and 90% matrix. The black curves correspond to 3CFdPS11 and the red curves dPS11. Solid curves are for additives in amPET and dashed curves are for additives in hPS.**

Table 1 shows typical values for the confidence limits to fit parameters obtained by Bayesian Inference (BI). The functional form used to describe the concentration dependence of the deuterated component was restricted to the region of the polymer film; therefore the fact that  $w_1$  exceeds  $h_1$  slightly implies a surface volume fraction at  $z = 0$  of somewhat less than 1, but does not have any impact on the air/polymer surface.

**Table 1. Fitted parameters and confidence limits using equation 2 for surface active blends 10% dPS11 or 3CFdPS11 in amPET.**

parameter	Fitted value		
	10% 3CFdPS11/amPET	10% dPS11/amPET	10% 3CFdPS11/hPS100
$h_1 / \text{nm}$	$9.9 \pm 0.9$	$9.7 \pm 1.6$	$11.7 \pm 4.2$
$w_1 / \text{nm}$	$11.0 \pm 0.3$	$11.2 \pm 1.0$	$12.3 \pm 3.2$
$h_2 / \text{nm}$	$143 \pm 5$	$111 \pm 5$	$29 \pm 9$
$w_2 / \text{nm}$	$72 \pm 4$	$63 \pm 6$	$12 (\pm 24)$

It appears that 3CFdPS11 in hPS100 has the highest surface concentration of any of the blended films, which is consistent with the high levels of surface hydrophobicity and lipophobicity seen in figure 2 for this combination, even at very low additive concentrations. However, it should be noted that the thickness obtained for the surface enriched layer,  $h_1$  (=11.7 nm) is only marginally greater than the depth resolution of the measurement, so values contain a significant error arising from this uncertainty and the choice of the functional form used to describe the concentration profile. What is more significant and unequivocally determined by the NRA experiments is the gradual variation in depth distribution apparent in the subsurface layer.

The dependence of the 3CFdPS11 depth profile on concentration in amPET is shown for spin cast blended films in Figure 7. Our results highlight the high level of surface activity in these blends, and in the case of the lowest concentration explored, the majority of the additive detected in the film appears to be present in the surface layer. Both the 5% and 10% additive blends yield similar results for the minimum concentration of additive adjacent to

the surface layer of approximately 0.4%, suggesting that this is a consistent measure of the binodal composition defining the upper solubility limit of 3CFdPS11 in amPET.

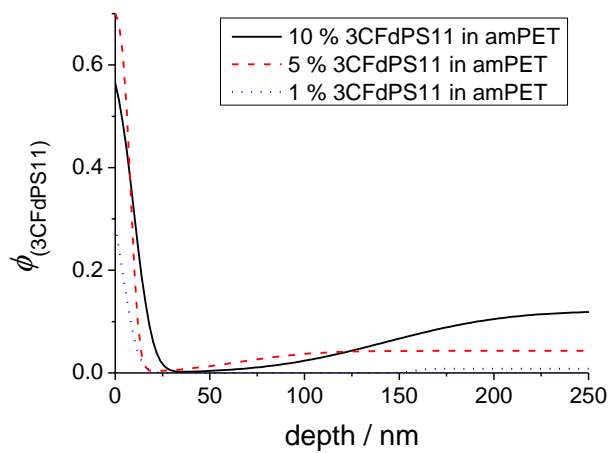


**Figure 7. Composition dependence of 3CFdPS11 in amPET films obtained by NRA.**

By integrating under the composition versus depth profile curves and correcting for the molecular volume of each polymer chain, we can estimate the surface excess,  $\Gamma$ , of adsorbed polymer chains per unit surface area to be

$$\Gamma = \frac{\rho h_s}{M_n} \quad (3)$$

where  $\rho$  is the density of the adsorbing species. Results for derived values of  $\Gamma$  obtained by nuclear reaction analysis are given in figure 8. Interestingly, for 10% mass fractions of polystyrene based additive, the surface excess was found to be quite similar, irrespective of fluorocarbon functionalisation and only weakly dependent upon matrix compatibility, provided that the blend is one in which the additive has some inherent surface activity.

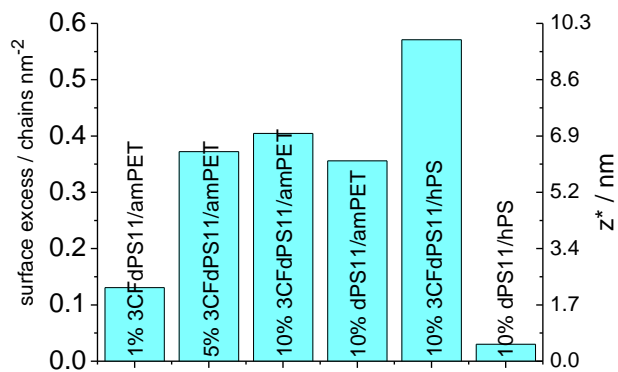


**Figure 8. Surface excess values for blended films.**

The composition profiles obtained are an average over the macroscopic area ( $\sim 20 \text{ mm}^2$ ) struck by the incident ion beam. Since the components of the polymer blend are chosen to be incompatible and expected to undergo phase separation in the bulk, it is not unreasonable to expect that there may also be lateral phase separation across the surface of a two-dimensional film. To explore this possibility further we conducted some AFM measurements on the higher concentrations of 3CFdPS 11 in amorphous PET. Figure 9 shows the variation in surface topography for a  $10 \times 10 \mu\text{m}$  scan carried out by AFM. At 15% 3CFdPS11, which was a higher concentration than we could obtain fittable neutron reflectometry data, evidence for surface dewetting was indeed seen by AFM. Before annealing, there appear to be small ( $< 5 \text{ nm}$ ) variations in surface height comprising a continuous layer with some sub-micron depressions within it. After annealing, the surface becomes considerably rougher and the cross-sectional analysis of the scan shown in figure 9b reveals features that regularly approach  $50 \text{ nm}$  in height. Analysis of larger ( $25 \times 25 \text{ micron}$ ) scans indicated that the r.m.s. roughness of the spin-cast samples was approximately  $1.8 \text{ nm}$ , and that this roughness increased to approximately  $11 \text{ nm}$  after annealing. However, because the vertical scale of roughness is very small compared to the lateral scale over which roughness is measured, the effective increase in surface area arising from roughness is miniscule, and amounts to relative increases in surface area of  $0.016\%$  and  $0.42\%$  for the unannealed and annealed samples respectively.

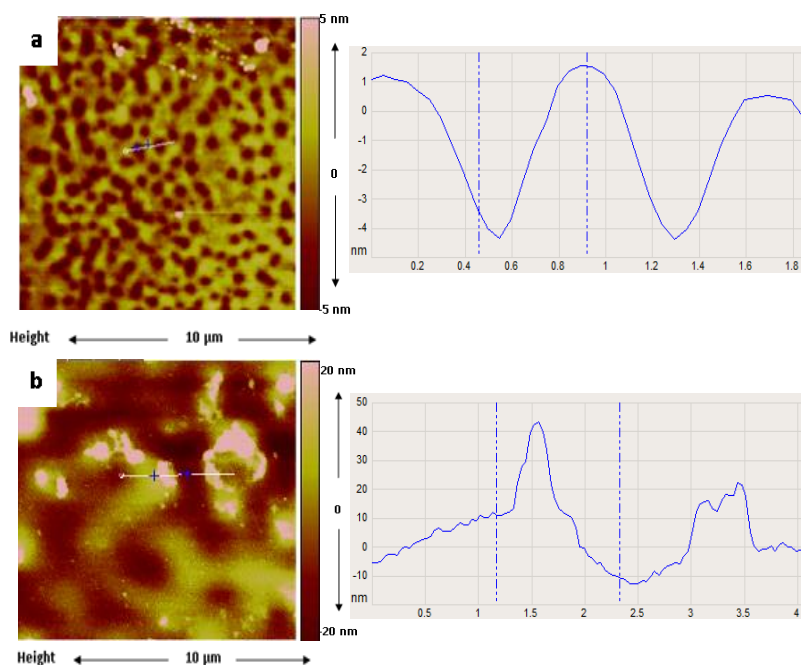


**Figure 9.** AFM height maps and cross sectional analysis for 15% 3CFdPS11 (a) before annealing and (b) after annealing at  $150 \text{ }^\circ\text{C}$  for 1 hour.

The influence of annealing on the precise nature of the surface enriched layer of 3CFdPS11 on amPET is beyond the resolution of ion beam analysis, so we used neutron reflectometry to explore this further. NR results for 10% 3CFdPS11 in amPET, before and after annealing are presented in figure 10(a) and reflectometry data were fitted using scattering length densities of  $2.43 \times 10^{-6} \text{ \AA}^{-2}$  and  $6.47 \times 10^{-6} \text{ \AA}^{-2}$  for amPET and dPS respectively according to

$$\phi = \phi_{dep} + \frac{\phi_s - \phi_{dep}}{2} \left( 1 + \operatorname{erf} \frac{h_1 - z}{w_1} \right) + (\phi_h - \phi_{dep}) \left( 1 + \operatorname{erf} \frac{z - h_2}{w_2} \right) \quad (4)$$

which has the same parameters as equation 2 except that the surface and depletion concentrations of 3CFdPS11,  $\phi_s$ , and  $\phi_{dep}$  are explicitly included. It is necessary to include  $\phi_s$  because the superior depth resolution of NR allows this parameter to be decoupled from  $h_1$ , whereas this would have led to over-parameterisation of the NRA data. We have also included  $\phi_{dep}$ , but fixed this parameter at the value obtained from NRA, which is more accurate for regions of the film where composition varies slowly with depth. Although NR is completely insensitive to the gradual increase in concentration with increasing depth beyond the depleted region<sup>31</sup> (figure 6), it is however superbly sensitive to the sharp gradients in the scattering length density profile associated with the adsorbed deuterated layer on the film surface. The dramatic change in R(Q) arising from annealing the sample seen in figure 10(a) can be attributed to the sharpening of the interface between the adsorbed 3CFdPS11 and the amPET-rich subphase apparent in figure 10(b). The very high (approaching unity) surface volume fraction of dPS, which is accurately resolved by NR is only possible with a complete surface wetting layer. In other words our NR analysis leaves very little scope for lateral inhomogeneity such as “islands” of different phases at lower concentrations, despite some evidence for this behaviour at higher concentrations apparent in the AFM results.

## Discussion

Our results show that high levels of surface modification arising from segregation of a surface active additive are possible in solution spin-cast blended films, regardless of the compatibility of the blend components. Our contact angle analysis results show that the characteristic surface properties of the blended films depend primarily on the surface energy of the additive material. It appears that the compatibility (or lack of compatibility) between the additive and the matrix in which it is dispersed is only of secondary importance to the surface properties. It is interesting to note that although the contact angle results with water and decane show a similar overall trend, the hydrophobicity with water appears to reach a plateau at lower concentrations than the lipophobicity with decane. The reason for this behaviour is not clear, although it appears to have little effect on the derived values

of surface energy, which do not change dramatically, except at the lower additive concentration range in figure 3 over which the film surface becomes more hydrophobic.

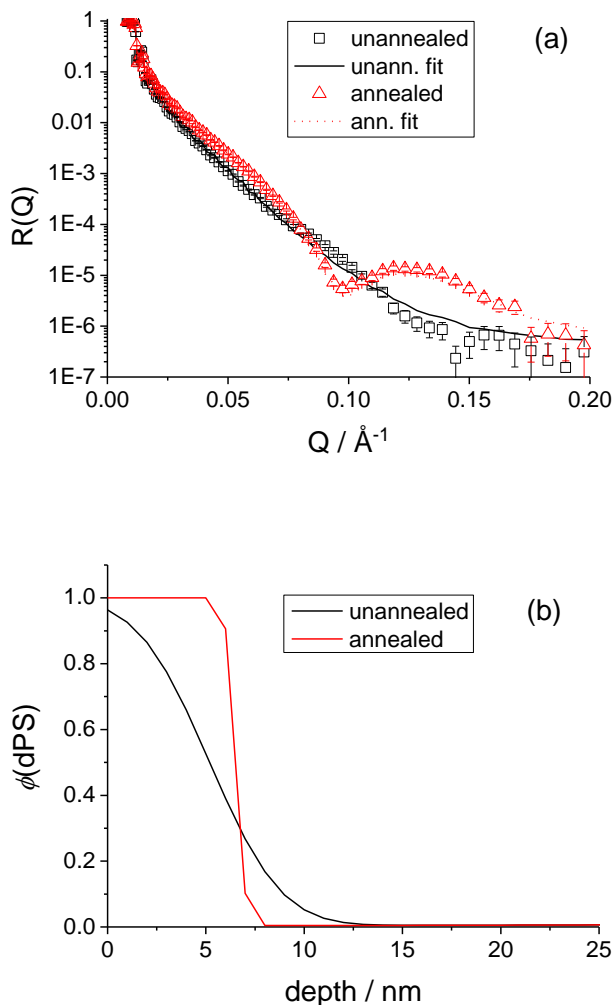


**Figure 10. Neutron reflectometry data and fits (a) and the corresponding composition versus depth profiles (b) for 10% 3CFdPS11 in amPET before and after annealing.**

Although it is possible that surface roughness can have significant impact on contact angle results, both AFM results for surface topography and contact angle results with n-decane confirm that roughness would have a minimal impact on the measured hydrophobicity or lipophobicity. Even the films that appear to show signs of dewetting (figure 9(b)) are relatively smooth in the sense that the increase in surface area over projected surface area (the relevant measure for Wenzel wetting) is of the order of 0.4 %. This is much too small to have any discernible impact on the measured contact angles, and we note that corresponding value for the unannealed sample was even lower; therefore we conclude that all of the spin-cast films can be treated as 'smooth' for the purposes of contact angle analysis.

The increase in surface roughness determined by AFM following annealing, albeit small has not previously been seen for similarly functionalised additives in compatible blends, and indicates that the surface enriched layer of functional polymer has a tendency to dewet the amPET-rich subphase. Under these circumstances the total amount of fluorocarbon functionalised material on the surface does not change, but the number of fluorocarbon groups exposed at the surface per unit area may in fact decrease. The absence of any loss in surface hydrophobicity following this coarsening of the surface might be attributed to a residual thin layer of 3CFdPS11 wetting the surface, or simply that the water droplets are effectively pinned by a continuous surface network of 3CFdPS11. Although we see no evidence for superhydrophobicity in any of our blended films, the fact that incompatibility appears to lead to greater levels of surface roughness is very interesting as this suggests that there may be a route towards superhydrophobic surfaces if the phase separation between the polymer components can be harnessed to generate similarly rough surfaces to those obtained by solution phase separation<sup>32</sup> or crystallisation<sup>33</sup> to achieve this effect.

It is interesting to note that while annealing does lead to significant increases in hydrophobicity and decreases in surface energy, both the fluorocarbon functionalised 3CFdPS11 and its unfunctionalised counterpart, dPS11, impart a significant level of hydrophobicity to amPET, even in the unannealed spin-cast films. This surface activity of 3CFdPS11 was evident, even in the blended stock solutions in toluene from which the films were prepared. When shaken, the stock solutions developed a short-lived, but appreciable level of foaming. Conversely, the stock solutions containing dPS11 did not foam when shaken, confirming the expected absence of surface activity of dPS11 (surface energy  $\sim 40 \text{ mJm}^{-2}$ ) in toluene (surface tension  $\sim 28 \text{ mJm}^{-2}$ ). On this basis, the spontaneous surface segregation of dPS in amPET from a toluene solution, before annealing, is quite unexpected; therefore we turn our attention to the ion beam analysis results which enable the surface phenomenology to be linked to the depth distribution of the components.

### ***Depth distribution of surface active components***

Remarkably, we find that for the 10% blends, the functional group has no dramatic effect on the total adsorbed quantity of additive, and indeed the increase in surface hydrophobicity of spin-cast dPS11 in amPET can clearly be seen to arise from a surface enriched layer of the dPS11 additive (figure 6). The implication of this surface excess, even before the dPS in amPET film has been annealed is that the polymers are able to undergo significant rearrangement during the later stages of the spin-coating process, when there is insufficient solvent present near the film surface to inhibit the segregation of the marginally surface active dPS11.

The insensitivity of the surface excess to functionality and incompatibility is most clearly illustrated in figure 8, where it is evident that there are approximately 0.4 additive polymer

chains per  $\text{nm}^2$  for all of the incompatible surface-active polymer blends where there is sufficient total additive present to provide this layer. Given our previous calculation<sup>10</sup> that 1  $\text{C}_8\text{F}_{17}$  group has an effective footprint of about  $0.5 \text{ nm}^2$ , it appears that up to 60% of the 3CFdPS11 incompatible blend film surface could be covered with fluorocarbon. Although we observe a slightly larger surface excess in the 3CFdPS11/hPS100 blend, it appears that incompatibility has little impact on the surface segregation, except when there is no other driver for segregation such as fluorocarbon functionalisation. The only blend which did not show this rather consistent level of surface segregation was the control dPS11/hPS100 blend, for which any extent of surface segregation was too small to resolve by ion beam analysis. The very small surface excess indicated by figure 8 is insignificant within the expected uncertainty.

For the surface active 3CFdPS11 blends, both the layer fits and the functional form fits (figure 4) are highly satisfactory, and show that a single model incorporating a surface enriched layer, a near surface region of reduced concentration and a bulk layer successfully capture the key features of all of the measured data, and the concentration profile is characteristic of a surface active polymer blended with a homopolymer with which it is only partially miscible.<sup>5</sup> The large peak near channel 1310 corresponds to the surface layer, which is highly enriched with the deuterium labelled 3CFdPS11. The data at higher channels correspond to the concentration of 3CFdPS11 deeper within the film, convolved with energy dependent nuclear reaction cross section. In figure 5, the incompatibility between the polystyrene based additives and the amPET matrix is clearly apparent in the form of the drastic depletion in composition centred at a depth of approximately 50 nm. Some depletion is also apparent, but to a far lesser extent, for the 3CFdPS11 in hPS blend, but this may be attributed to the incomplete equilibration of the surface excess layer rather than significant incompatibility between the blend components.

The 'steps' in the simulation that arise from the sudden changes in composition in the layer model are not apparent in the data the resulting layer fit has a slightly higher partial chi-squared values than were obtained for the analytical functional form. Although this improvement to the fit with the functional form model is welcome, what is more significant is that this was achieved with just 5 parameters, (see table 1) as opposed to the 9 parameters that were necessary to fit 4 finite layers and one thick layer. While it is possible to approximate such a function by a large number of thinner layers, each layer adds as many parameters to the analysis as there are components in the material. (There are  $n-1$  degrees of freedom introduced by  $n$  components per layer since the total volume fraction must add up to unity plus one degree of freedom due to the variable layer thickness.) Given that there is no evidence that the expected functional form is incompatible with the NRA data, Ockham's Razor impels us to reduce the free parameters of the fitting by imposing the functional form on the data.

As well as being more physically reasonable since the expected smooth profile is obtained, and preferable since fewer parameters are required, our analysis shows further benefits of the analytical functional form over the layer model in fitting the NRA data. It is noticeable from figure 4 that the quality of fit for the functional form is also better in the region of very low scattering intensity between the surface excess and the bulk concentration. This is because the model is manifestly valid, and the spectral shape in the low intensity region is determined (correctly) from the shape in the adjoining high intensity regions. The width of the second interface,  $w_2$ , between the depleted region and the bulk material can yield important insights into the physical nature of the blends. For miscible polymer blends, the interfacial width can be used to estimate the diffusion coefficient of the additive.<sup>34</sup> In this case, where the polymers are quite immiscible in the dry film, the interfacial width is a function of the interaction parameter between the polymer components. However, this parameter is more directly obtainable from the minimum in concentration between the surface excess and the bulk composition if we assume that it is close to its equilibrium composition. Allowing for the possibility for further demixing, the minimum concentration measured by ion beam analysis yields an upper limit to the miscibility of the additive in the matrix, i.e. the binodal composition.<sup>5</sup> Using Flory-Huggins theory, we can estimate the strength of the unfavourable interactions between the PET matrix and the dPS additive. If we assume that the amPET is best described by the weight-average molecular weight, we obtain an effective Flory-Huggins interaction parameter,  $\chi_{(dPS-amPET)}$ , of 0.035 with respect to a reference volume of  $200 \text{ \AA}^3$ ; the geometric mean of the repeat unit volumes of each polymer. Furthermore, we can estimate that the binodal at the dPS-rich side of the phase diagram would be approximately  $\phi(amPET)=10^{-6}$ . Although we should treat these derived values with considerable caution, it is reasonable to conclude that the 3CFdPS11 is only very sparingly dispersible in the amPET matrix, and that it is likely that amPET is even less soluble in the corresponding 3CFdPS11-rich phase. This prediction is supported by our neutron reflectometry analysis of the influence of annealing on the surface segregation of 3CFdPS11 on amPET. It is noticeable that the total adsorbed quantity,  $z^*$ , given by the integral under the composition profile only increases slightly with annealing, and that the major difference observed is in the sharpening of the interface between the adsorbed layer and the amPET rich layer beneath it. Furthermore, it appears that in the annealed sample, the amPET matrix is almost entirely excluded from the adsorbed 3CFdPS11 surface layer and vice-versa. We note that this sharp interface between the adsorbed layer and the amPET sub-phase may reduce the mechanical robustness of the interface. Our previous experiments indicate that when comparable length functionalised PMMA is compatible with the matrix, it is quite stable with respect to abrasion in water, but less so with acetone.<sup>35</sup> However, for maximum mechanical stability, brush-like layers need to be well-entangled with the subphase,<sup>36</sup> which is not possible for PS materials of this molecular weight, particularly with an incompatible matrix.

From the practical point of view the binodal composition of additive in the polymer matrix is important to characterise accurately as it defines the minimum concentration required to achieve the maximum equilibrium surface excess. For a thick film of amPET our analysis indicates that just 0.4% 3CFdPS11 would be required in the bulk to be in equilibrium with a saturated surface layer of this additive. (Results for the analytical function fits to both the 5% blend and the 10% blend give very similar values.) However, to achieve such a spectacular efficiency of surface modification from such a low average bulk loading of additive requires a high proportion of the additive buried within the film to be able to migrate to the surface. With the knowledge of the surface excess concentration and minimum bulk loading it is straightforward to estimate the mobility required under typical process conditions. For 3CFdPS11 in amPET, the adsorbed surface excess layer would be approximately 6 nm thick. At 0.4 % bulk loading of additive, it would require all of the 3CFdPS11 in the uppermost 1.5 microns of film to migrate to the film surface to create such a surface excess. On a production line, blend additives can only migrate to the film surface during the limited period of time that the film is held above its glass transition temperature. In a typical process, this time might be less than one minute; therefore we can estimate that the minimum diffusion coefficient required to achieve surface modification is approximately  $3 \times 10^4 \text{ nm}^2 \text{ s}^{-1}$ . Although we have not measured the diffusion coefficient in amPET due to the very low solubility of the 3CFdPS11 additive, we note that this diffusion coefficient is of the order that would be predicted for tracer diffusion of dPS11 in PS by WLF calculations at approximately 200 °C.<sup>37</sup> While this temperature is not unreasonable for film processing conditions, it should be noted that it comes close to the limit of thermal stability measured for this type of additive.

## Conclusion

We have shown that in solution cast films, it is possible for extremely efficient surface modification to occur in a blended film, even when the surface active additive is quite incompatible with the matrix polymer. It is apparent that when the blend components are incompatible, even a marginal preference for one component to locate at the film surface over another leads to a complete wetting layer of that component, and surprisingly this occurs even without annealing above the glass transition temperature. From this we conclude that the blend components are able to reorganise according to their marginally different surface energies even in the presence of a solvent which has a lower surface energy than either polymeric component. The more strongly surface active fluorinated additive gives rise to similar levels of hydrophobicity and lipophobicity, regardless of its compatibility with the matrix.

Ion beam analysis (IBA) allows the direct determination of the vertical composition profiles which reveal how the additive surface segregation contributes to the hydrophobicity and lipophobicity observed by contact angle analysis. Further, IBA facilitates data interpretation

which fully parameterises the system, using both a reasonable chemical model of immiscibility and a chemical (molecular, not elemental) description of the binary system. This in turn facilitates the use of Bayesian methods to extract parameter uncertainties, given the Flory-Huggins model. The data themselves affirm the validity of the functional form of the depth profile, and since this function can be validly imposed on the data the function parameters are all determined by the whole dataset with a consequent improvement in precision. More information can be extracted from the data, given a model, and here we have been able to infer further valuable information on the system, including the Flory Huggins interaction parameter and the minimum additive concentration likely to be required in a bulk coating of these components. This parameterisation of the extent of incompatibility is further supported by our neutron reflectometry analysis of the fine structure of the surface enriched layer of 3CFdPS11 which was found to become highly segregated from the amPET subphase with a very narrow interface between these phases after annealing. This detailed analysis enables estimation of the minimum combination of processing time and temperature necessary to populate achieve surface modification by an additive migrating to a film surface.

## Acknowledgement

We thank DuPont Teijin Films, Durham University and the Technology Strategy Board for support of this work via Knowledge Transfer Partnership 8131 and are grateful to STFC for provision of the neutron reflection facilities at ISIS.

## References

- (1) Lopez-Donaire, M. L.; Santerre, J. P. *Journal of Applied Polymer Science* **2014**, *131*, 15.
- (2) Avilova, V. S.; Barkovskaya, O. A.; Kudashev, S. V.; Rakhimova, N. A.; Shevchenko, K. R.; Zheltobryukhov, V. F.; UNIV VOLG TECH (UYVL-Soviet Institute): 2013, p 0.
- (3) Hutchings, L. R.; Narrainen, A. P.; Thompson, R. L.; Clarke, N.; Ansari, I. *Polymer International* **2008**, *57*, 163.
- (4) Hardman, S. J.; Hutchings, L. R.; Clarke, N.; Kimani, S. M.; Mears, L. L. E.; Smith, E. F.; Webster, J. R. P.; Thompson, R. L. *Langmuir* **2012**, *28*, 5125.
- (5) Ansari, I. A.; Clarke, N.; Hutchings, L. R.; Pillay-Narrainen, A.; Terry, A. E.; Thompson, R. L.; Webster, J. R. P. *Langmuir* **2007**, *23*, 4405.
- (6) Narrainen, A. P.; Hutchings, L. R.; Ansari, I.; Thompson, R. L.; Clarke, N. *Macromolecules* **2007**, *40*, 1969.
- (7) Paul, D. R. *Advances in Chemistry Series* **1986**, *3*.
- (8) Esteves, A. C. C.; Lyakhova, K.; van der Ven, L. G. J.; van Benthem, R.; de With, G. *Macromolecules* **2013**, *46*, 1993.
- (9) Esteves, A. C. C.; Luo, Y.; van de Put, M. W. P.; Carcouet, C. C. M.; de With, G. *Adv. Funct. Mater.* **2014**, *24*, 986.
- (10) Hutchings, L. R.; Narrainen, A. P.; Eggleston, S. M.; Clarke, N.; Thompson, R. L. *Polymer* **2006**, *47*, 8116.
- (11) Kurokawa, K.; Yamashita, K.; Doi, Y.; Abe, H. *Polym. Degrad. Stabil.* **2006**, *91*, 1300.

- (12) Rysz, J.; Bernasik, A.; Ermer, H.; Budkowski, A.; Brenn, R.; Hashimoto, T.; Jedlinski, J. *Europhysics Letters* **1997**, *40*, 503.
- (13) Geoghegan, M.; Jones, R. A. L.; Clough, A. S. *Journal of Chemical Physics* **1995**, *103*, 2719.
- (14) Bruder, F.; Brenn, R. *Physical Review Letters* **1992**, *69*, 624.
- (15) Jones, R. A. L.; Norton, L. J.; Kramer, E. J.; Bates, F. S.; Wiltzius, P. *Physical Review Letters* **1991**, *66*, 1326.
- (16) Lee, Y.; Han, S.; Lim, H.; Jung, H.; Cho, J.; Kim, Y. *J. Adhes. Sci. Technol.* **2001**, *15*, 1079.
- (17) Elman, J. F.; Johs, B. D.; Long, T. E.; Koberstein, J. T. *Macromolecules* **1994**, *27*, 5341.
- (18) Bucknall, D. G. *Progress in Materials Science* **2004**, *49*, 713.
- (19) Jinnai, H.; Kitagishi, H.; Hamano, K.; Nishikawa, Y.; Takahashi, M. *Physical Review E: Statistical, Nonlinear, and Soft Matter Physics* **2003**, *67*, 021801/1.
- (20) Moffitt, M.; Rharbi, Y.; Tong, J.-D.; Farhina, J. P. S.; Li, H.; Winnik, M. A.; Zahalka, H. *Journal of Polymer Science, Part B: Polymer Physics* **2003**, *41*, 637.
- (21) Geoghegan, M. In *Conference on Polymer Surfaces and Interfaces III*; Richards, R. W., Peace, S. K., Eds.; John Wiley & Sons Inc: Durham, England, 1997, p 43.
- (22) Composto, R. J.; Walters, R. M.; Genzer, J. *Materials Science and Engineering R* **2002**, *R38*, 107.
- (23) Binks, B. P.; Fletcher, P. D. I.; Sager, W. F. C.; Thompson, R. L. *Langmuir* **1995**, *11*, 977.
- (24) Chiu, H. J. *Polymer Engineering and Science* **2007**, *47*, 2005.
- (25) Owens, D. K.; Wendt, R. C. *Journal of Applied Polymer Science* **1969**, *13*, 1741.
- (26) Payne, R. S.; Clough, A. S.; Murphy, P.; Mills, P. J. *Nuclear Instruments & Methods in Physics Research Section B- Beam Interactions with Materials and Atoms* **1989**, *42*, 130.
- (27) Barradas, N. P.; Jeynes, C.; Webb, R. P. *Applied Physics Letters* **1997**, *71*, 291.
- (28) Moller, W.; Besenbacher, F. *Nuclear Instruments & Methods* **1980**, *168*, 111.
- (29) Kimani, S. M.; Thompson, R. L.; Hutchings, L. R.; Clarke, N.; Billah, S. M. R.; Sakai, V. G.; Rogers, S. E. *Macromolecules* **2014**, *47*, 2062.
- (30) Jones, R. A. L.; Kramer, E. J.; Rafailovich, M. H.; Sokolov, J.; Schwarz, S. A. *Physical Review Letters* **1989**, *62*, 280.
- (31) Thompson, R. L.; Hardman, S. J.; Hutchings, L. R.; Narrainen, A. P.; Dalglish, R. M. *Langmuir* **2009**, *25*, 3184.
- (32) Huang, Y. F.; Liu, X. H.; Zhang, F. F.; Dong, J. F.; Luo, Y. B.; Huang, C. *Polym. J.* **2013**, *45*, 125.
- (33) Lu, X. Y.; Zhang, C. C.; Han, Y. C. *Macromol. Rapid Commun.* **2004**, *25*, 1606.
- (34) Clarke, C. J.; Jones, R. A. L.; Clough, A. S. *Polymer* **1996**, *37*, 3813.
- (35) Thompson, R. L.; Narrainen, A. P.; Eggleston, S. M.; Ansari, I. A.; Hutchings, L. R.; Clarke, N. *Journal of Applied Polymer Science* **2007**, *105*, 623.
- (36) Norton, L. J.; Smigolova, V.; Pralle, M. U.; Hubenko, A.; Dai, K. H.; Kramer, E. J.; Hahn, S.; Berglund, C.; Dekoven, B. *Macromolecules* **1995**, *28*, 1999.
- (37) Karim, A.; Mansour, A.; Felcher, G. P.; Russell, T. P. *Physical Review B* **1990**, *42*, 6846.
- (38) Jeynes, C.; Barradas, N. P.; Rafla-Yuan, H.; Hichwa, B. P.; Close, R. *Surf. Interface Anal.* **2000**, *30*, 237.

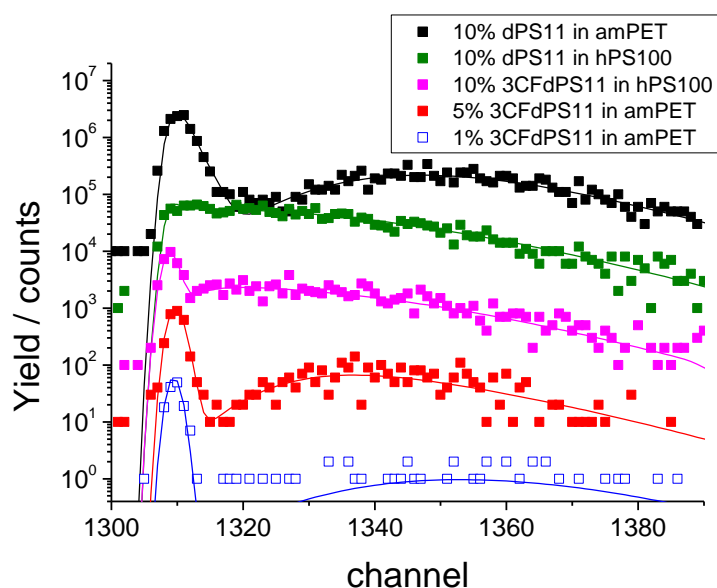
## Supporting Information

### S.I.1.

Datafurnace fitting was carried out using the reaction cross-sections of Möller and Besenbacher<sup>28, 25</sup> where NDF implements the anisotropy coefficients tabulated in this paper. The depth scale was calibrated to nanometers by assuming ideal mixing and densities of 1.38 and 1.10 g/cm<sup>3</sup> for amPET and dPS respectively. The fitted parameters were extracted together with an estimate of their uncertainty given by Bayesian inference methods.<sup>30</sup>

Note that fitting the IBA data for these binary mixtures is able to use *molecules* (not elements, that is, involving only two and not five or more parameters) to specify composition<sup>38</sup>. The experimental protocols for obtaining comparable ion beam analysis and neutron reflectometry experiments has been well established for other similar types of sample in our earlier work.<sup>5</sup>

### S.I.2



S.I.1. NRA proton yield and DataFurnace fits using equation 2 for functional PS in hPS or amPET corresponding to the profiles shown in figure 6. Data have been offset by successive decades for clarity.